



Experimental and theoretical study on the charge transfer between polyaniline and single walled carbon nanotubes

Saoudi M.¹, * Ajjel R.¹, Zaidi B.^{2,3}

¹Laboratoire des Energies et de Matériaux (LabEM), Ecole Supérieure des Sciences et de Technologie de Hammam Sousse. Sousse University, Tunisia.

²Unité de Recherche, Matériaux nouveaux et Dispositifs Electroniques Organiques, Faculté des Sciences de Monastir, 5000 Monastir University, Tunisia.

³Department of Physics, Faculty of Sciences Ad-Dwadimi, P.O. Box 1040 Ad-Dwadimi 1191, Shagra University, Saudi Arabia.

Received 15 Apr 2016, Revised 14 Sep 2016, Accepted 22 Sep 2016

*Corresponding author. E-mail: mariem_saoudi@yahoo.fr; Phone: +216.73.370.711; Fax: +216.73.370.710

Abstract

Polyaniline emeraldine base (PANI_EB) is doped with sulfonic acid in Dimethyl formamide (DMF) solvent and mechanically functionalized with single walled carbon nanotubes (SWCNTs). In this paper, a systematic vibrational and optical properties study is reported as a function of SWCNTs weight concentration. Also, Fourier transform infrared (FTIR) analysis and optical absorption (OA) measurements were achieved. Our aim is to evaluate the functionalization process between both components and to elucidate the corresponding changes on the optical properties. In this context and to support the charge transfer from doped polyaniline to carbon nanotubes, analogous theoretical study based on Density Functional Theory (DFT) is carried out. This study is based on the optical and vibrational calculations. Principally, spin density distribution, atomic charge and bond length modifications from ground to oxidized state are used to supports the grafting process. The correlation structure-properties obtained either experimentally or theoretically evidences that the resulting composite exhibits good photovoltaic properties.

Keywords: Polyaniline emeraldine base, Single Walled Carbon Nanotubes, Density Functional Theory, Charge Transfer, Photovoltaic Cells.

1. Introduction

Organic materials are in our days the most promising candidates for the use as active layers in the future of electronic devices manufacturing, due to their interesting electro-optical properties [1-3]. As it is widely known, fragility and operating life time are both handicaps for electronic organics devices. To overcome these handicaps, the added small amount of carbon nanotubes leads not only to a good mechanical strength [4] but also in higher operating life time [5]. Particularly, for photovoltaic applications, the good dispersion of carbon nanotubes in the polymer matrix leads not only to the charge transfer but also to better transport properties via their good electron-hole mobilities [6]. This charge transfer occurs because the overlapping between the electron diffusion length and the distance separating the photo-generation sites and nanotubes. Physically, the charge transfer creation involves generally the creation of additional absorption features in the visible region and results in a good compatibility with the solar spectrum [7]. In fact, the resulting interpenetrating network results in

higher charge separation and good collection efficiencies due to the formation of bulk P-N hetero-nanojunctions [8-10].

Among of conducting polymers, polyaniline (PANI) is the most highly studied due to its varied chemical and physical properties [11-13]. The particular interest restricted to this material is the consequence of good environmental stability and easily synthesis [14-17]. A simple chemical treatment of PANI leads to new oxidation degree where its conductivity can be reversibly switched between electrically insulating and conducting forms [18]. The fully oxidized (reduced) form is named as pernigraniline base PNB, (leucoemeraldine base LB). Then, if nitrogen atom is half oxidized, PANI is in emeraldine base form (EB; form) [19].

Although, some systematic studies involving PANI have been published, few papers have been devoted to the possibility of its integration as active layers in photovoltaic devices under its different doped or undoped forms [20]. Therefore, it is of interest to study the modification of their properties upon acid doping and after its functionalization with carbon nanotubes. For that and in order to specify the appropriate applications, correlation structure-properties should be established either experimentally or theoretically [21–25]. Indeed, quantum calculations based on density functional theory (DFT) are the most appropriate tools to describe the organic materials properties [23, 26, 27]. These calculations permit to give some informations which are experimentally inaccessible and permits to predict the applicability field [27, 28]. Then, as a consequence of data processing development, calculations using large scale basis set and a large number of repeating units are currently possible [26, 27].

In this work a combined experimental and theoretical investigation on the composite based on doped polyaniline and single walled carbon nanotubes (SWCNTs) is presented. Our aim is to establish a correlation structure-properties after carbon nanotubes adding and to evaluate possible applications based on the observed optical and vibrational properties changes. Experimental optical absorption and FTIR measurements are used to evaluate changes on the optical and vibrational properties. Moreover, a systematic theoretical study based on DFT quantum calculations is presented in order to elucidate the polymer functionalization process with SWCNTs and to evaluate the parameter of the photovoltaic cell that can be fabricated from. Particularly, the charge transfer properties and the corresponding electronic structure are of great interest.

2. Experimental and computational details

2.1. Preparation of the nano-composite

Polyaniline emeraldine base and single walled carbon nanotubes were purchased from Sigma-Aldrich. The polyaniline powder (purity of 99.99%) has the number average molecular weight of Mn > 15000 and a refractive index of 1.85, a melting point higher than 600 K, and a density of 1.36 g/ml at 300K. Then, the SWCNTs were produced by electric arc technique and have diameter varying from 1.0 nm to 1.2 nm and a length of nearly 500 nm. The classical procedure used for the doping process is similar to that previously reported by A. G. MacDiarmid et al. [29]. First, the powder was placed for 2 hr in a mixture made up of 20% of sulfonic acid (R-SO₃H) and 80% of DMF. Then, the doped polyaniline powder was washed three times by DMF. In fact, treating polyaniline with sulfonic acid having the molarity of 1.0, is principally done in order to obtain the conducting form of polyaniline (emeraldine salt) and to facilitate the grafting process between both components.

The procedure used to prepare the composite is based on the direct mixture of both components as it is previously described [7]. The PANI at doped states is dissolved in DMF solvent and SWNTs are mechanically dispersed in the same solvent for three hours in two separate recipients. This step is immediately followed by a sonication process for 30 min and by applying centrifuges forces. When the SWCNTs dispersion is achieved, the polyaniline solution is progressively added by a quantitative amount to the already dispersed SWCNTs in order to obtain the appropriate SWCNTs weight concentration. After SWCNTs dispersion, five SWCNTs weight concentrations are obtained (0%, 0.71%, 1.16 %, 2.1 %, and 5 %). These concentrations are chosen to be lower than 5%, principally to overcome Van der Walls cohesive forces in order to obtain a good dispersed

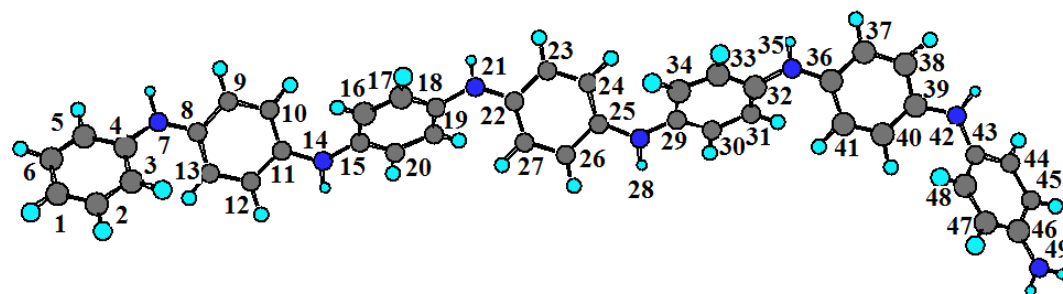
SWCNTs state [30, 31]. The obtained solution relative to each SWCNTs concentrations were deposited at room temperature with nearly uniform thickness on silica and KBr pellets respectively for optical absorption and infrared analysis. For optical absorption measurements, all substrates were cleaned in ultrasonically bath with deionized water and ethanol. The composite film obtained after solvent evaporation is introduced in an oven and is subsequently heated under vacuum at the temperature of 390 K for about 1 h.

2.2. Experimental measurements

Infrared absorption measurements are recorded using a Bruker Vertox 80 V interferometer with the resolution of 4 cm^{-1} . The samples were pellets of KBr painted with the organic compound under study [32]. For each SWCNTs weight concentration and in order to eliminate the effect of residual solvent and the KBr, the reference of measurement is obtained by carrying out both infrared spectrum of the KBr alone and those of KBr mixed with the DMF. The optical absorption spectra are recorded using UV1800 spectrophotometer working in the absorption mode with the wavelength varying from 200 nm (6.2 eV) to 2000 nm (0.62 eV).

2.3. Theoretical details

Concerning the theoretical part, all the structures including PANI at neutral or doped states and at different chain lengths, SWCNTs and the resulting nano-composite have been fully optimized using the most popular Becke's three-parameter hybrid functional, B_3 [33], with non-local correlation of Lee-Yang-Parr, LYP, abbreviated as B3LYP method [34, 35] without constraint. Theoretically, the PANI doping process is accomplished by adding (removing) electrons to (from) the corresponding modeling structure at its neutral state. For the polyaniline at both neutral or doped state calculations are done for different chain length (the fragments number i (atoms labeled from 0 to $7i$ in scheme 1)) Optical absorption spectra were calculated using the time-dependent density functional theory (TD-DFT) method with the 6-31G (d) basis set which is widely applied to organic polymers [35-39] and were fitted to Gaussian curves within Swizard program [36]. Vibrational frequencies calculations have been carried out with DFT at 6-31G* level method [28, 37, 38] after the ground state optimization. The Highest Occupied Molecular Orbital (HOMO), the Lowest Unoccupied Molecular Orbital (LUMO) levels and the HOMO-LUMO gap are deduced from these calculations [39]. The electron density iso-contours plots at the ground states are obtained by the optimization using TD-B3LYP6-31G (d) method. These calculations were performed by the Gaussian 09 package [40].



Scheme1: Molecular structure of polyaniline. Nitrogen (7, 14, 21, 28, 35, 42 and 49) and Carbon atoms are labeled with their number for the optimization in both neutral and doped states.

3. Results and discussions

Figure 1 represents changes of FTIR spectra of PANI/SWCNTs composites as a function of SWCNTs weight concentration. Band positions and assignments are referred to the already published vibrational studies [41, 42]. All spectra are normalized by referring to the band at 1124 cm^{-1} which represent ring deformation and have not been affected when SWCNTs are added.

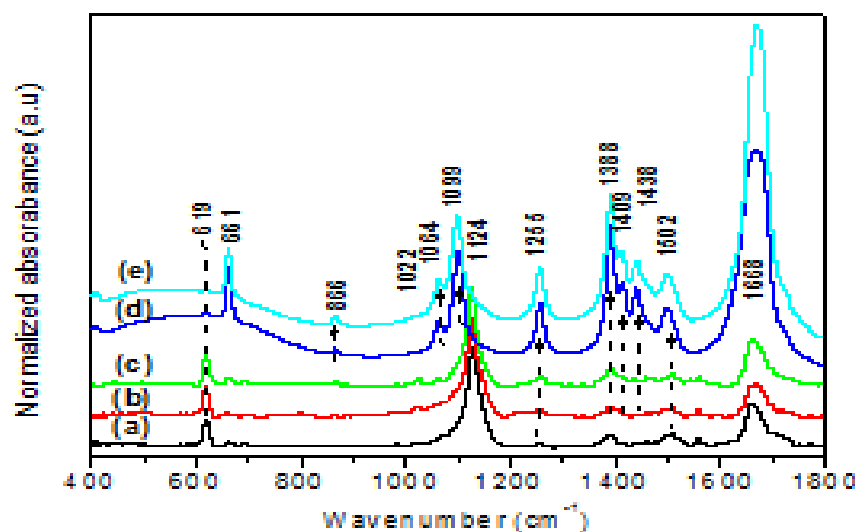


Figure 1: FTIR Spectra of polyaniline functionalized with SWCNTs as a function of SWCNTs concentration (a) 0%, (b) 0.71%, (c) 1.16 %, (d) 2.1 %, and (e) 5 %.

For SWCNTs concentrations lower than 2.10%, there are no significant changes in the shape of FTIR spectra, at least the increase of the band situated at 619 cm^{-1} , attributed to the C-N deformation. At these concentrations there is a conformational change due to SWCNTs inserting but without covalent functionnalization process. Starting from 2.1 % SWCNTs weight concentration, the spectrum is severely affected. New band appears at 1255 cm^{-1} , traducing the covalent binding between both components. Moreover, both bands at 1124 cm^{-1} and at 619 cm^{-1} are respectively shifted to 1099 cm^{-1} and to 661 cm^{-1} . These oscillations frequencies shifts and the netter intensity increase of the last band at 661 cm^{-1} , indicate a new molecular arrangement due to the SWCNTs inserting [43].

In the other hand, the weak band situated at 1022 cm^{-1} ascribed to the C-H deformation disappears and a news band appears at 1062 cm^{-1} . Then, bands situated in the range 1350 to 1700 cm^{-1} are severely affected by referring to those relative to the basic material. Indeed, bands at 1388 cm^{-1} and at 1502 cm^{-1} and 1688 cm^{-1} respectively attributed to C-H binding, ring deformation and N-H switching are dramatically improved in intensity supporting the aromaticity increase of the resulting compound. Two other new bands appear at 1409 and at 1438 cm^{-1} which traduce covalent binding between both components via new C-N link [44]. In fact, the appearing of new vibrational frequencies and the disappearing of another demonstrate that there is a covalent functionnalization process [45]. It is of importance investigate this functionnalization process which is the major factor to evidence to electro-optical properties of the resulting composite. As carbon nanotubes are generally donating moieties, if there is a covalent functionnalization process, polyaniline at doped state will be oxidized. For these reason a re-optimization process and the same calculations are done on the already optimized doped polyaniline structure to reach the oxidized state. Starting from this point of view, figure 2 represents the normalized infrared spectra obtained either experimentally or theoretically of the doped state by referring to those of oxidized state.

In fact, these theoretical calculations are done to support in a first step the molecular structure of the basic material and to elucidate the change from neutral to the oxidized state which can check the reactive sites for an eventual grafting process [7]. Indeed, from the experimental to the theoretical spectrum, all vibrational frequencies are found with nearly same intensities and positions except a shifting of maximum 90 cm^{-1} is observed for the band at 1124 cm^{-1} which represent ring deformation. This shifting is essentially due to the fact that calculations are done in gaseous phases and without inter-chain interactions [7].

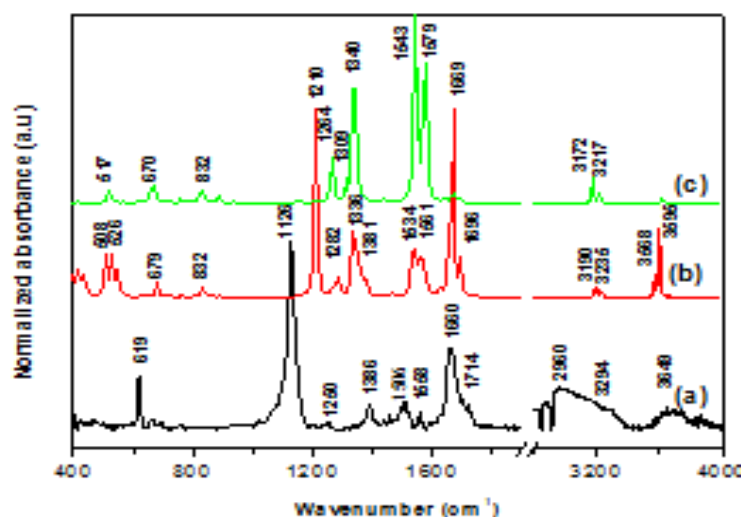


Figure 2: Infrared spectra of doped polyaniline, (a) experimental, (b) theoretical and (c) doped polyaniline after oxidation (c).

Particularly, hindrance effects which are necessarily dominant in the real material are evidently absent on the modeling structure reported in scheme 1, especially for the ring deformation that appears at 1124 cm^{-1} . From doped polyaniline to its oxidized state there are some changes. First, bands at 1207 cm^{-1} (ring vibration) and at 1667 cm^{-1} (NH_2 -switching) disappear simultaneously with the appearance of a new band at 1309 cm^{-1} . In the other hand, bands at 1543 and at 1570 cm^{-1} attributed to the symmetric and anti-symmetric C-H binding are improved similarly to those situated at 3190 cm^{-1} and at 3217 cm^{-1} . However, the band at 3595 cm^{-1} is severely quenched. These changes are principally due to the creation of quinoidal form of polyaniline [46, 47].

Figure 3 represents bond length, atomic charges modifications from the neutral to the oxidized states and the resulting spin density. Atoms are numbered in scheme 1, and bond length number n represents distance between neighboring atoms n and n+1. As shown, for the bond length variations, the most changes are nearly repetitive and concerns bonds which are directly related to the nitrogen atom and/or to their directly bonded carbon atoms.

In fact the oxidation process is followed by a new electronic repartition due to the new conformation as it is represented in figure 3 which induces the appearing of quinoidal form [46]. As shown, before the oxidation process, the higher atomic charges are restricted to nitrogen atoms numbered as 7, 14, 21, 28, 35, 42 and 49. Then, after oxidation, the most changes are restricted for these sites and their neighboring atoms which exhibit a more higher atomic charge. In the other hand, the resulting spin density distribution (figure 3-c), demonstrates also for doped PANI, only nitrogen atoms exhibits higher spin density. These first preliminary results let to conclude that the reactive sites are located around the nitrogen atoms.

As, it is shown, changes of vibrational frequencies are limited around the nitrogen atoms in the polymer skeleton. These results are in good agreement with the observed changes in atomic charges and in the geometric parameters. Therefore, the most probable site of interaction for which carbon nanotubes can be grafted is the nitrogen atoms. This result was already supported by a systematic SERS and FTIR experimental study on the neutral PANI/SWCNTs composite [42]. As it is known, carbon nanotubes have unique electronic properties [48], and the already proposed grafting mechanism are checked by electronic changes involving C=C groups which constitutes the tube [7]. Our modeling structure of the nano-composite is based on the covalent bonding between both components (figure 4). It is of importance to note that, the non-covalent bonding can be also present on the final structure. These non-covalent bonding are due to the intensive Van der Walls cohesive Force for carbon nanotubes which inhibit the homogenous dispersions process [30, 31].

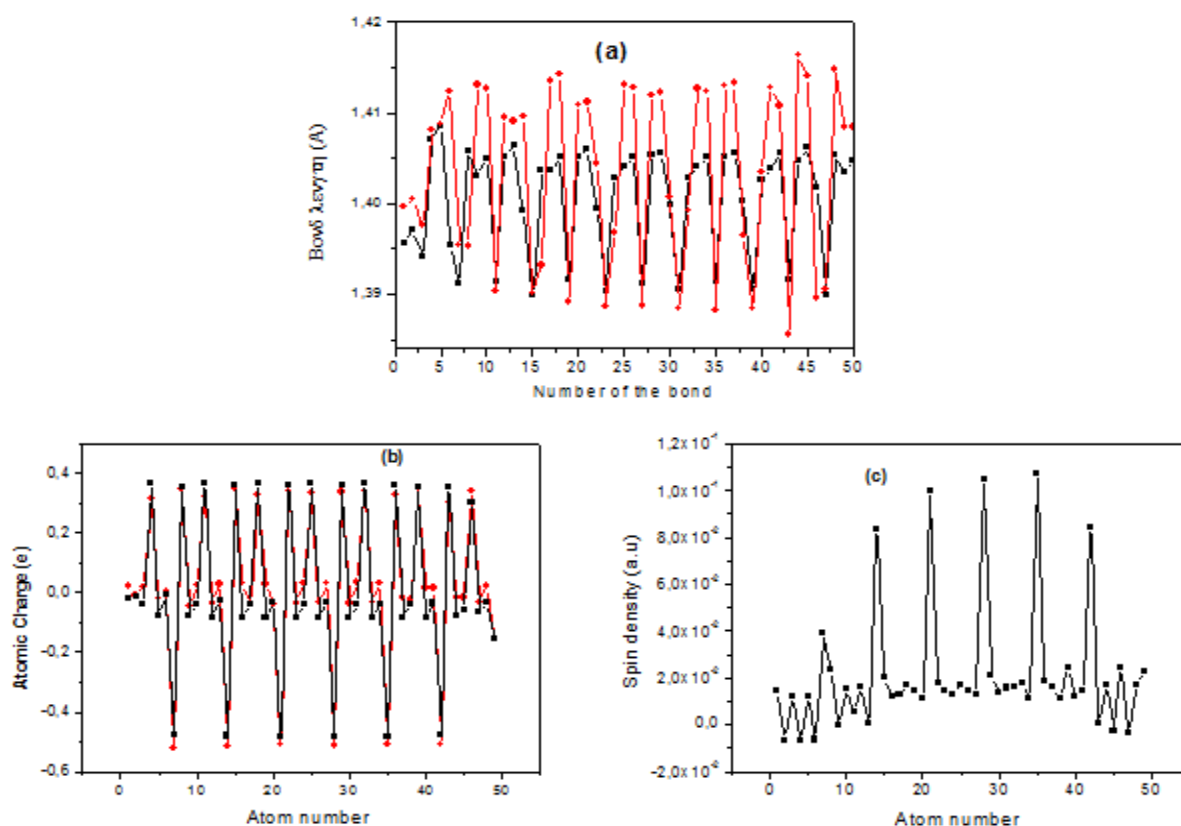


Figure 3: Changes of bond length (a), of atomic charge (b) from doped (■) to the it's oxidized state (●) and the resulting spin density at the doped state (c).

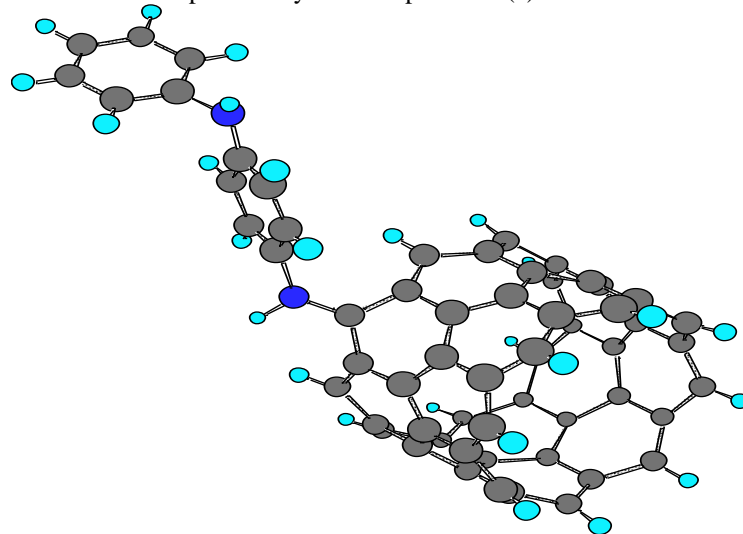


Figure 4: Modeling structure of the nano-composite D-PAN/SWCNTs.

To support this hypothesis, figure 5 represents the change of optical absorption spectra after doping and after SWCNTs adding obtained either experimentally or theoretically. From this figure, same transitions are found and a decrease of the optical gap after doping and after SWCNTS adding is clearly seen in both cases

which support the already proposed grafting mechanism. From experimental to theoretical spectra, we it is noted that band intensities of theoretical spectra are more pronounced. This difference is principally due to the fact that calculations are done on the modeling structure already presented in figure 4, for which the SWCNTs concentration is higher than that used in experimental part. Moreover, experimentally, the doping process is accomplished via adding acid entities which leads to the molecular structure modification. Theoretically the process is accomplished only by electron adding. As it is demonstrated for PANI at its neutral state, the $\pi-\pi^*$ transition which dominates the energy gap is maximized at 290 nm and the corresponding energy gap is 3.75 eV. The other transitions at higher energy (lower wavelength) are however attributed to $\sigma-\sigma^*$ and $\sigma-\pi^*$ transitions [49]. For the doped polyaniline, a large band is created giving rise to the optical gap decrease. This gap reduction is due to the π -polaron and/or and polaron- π^* band transitions [50]. This new band results on the decrease of the optical gap at the onset of nearly 2.63 eV. When SWCNTs are added, the spectrum is dramatically changed and a new band appears at $\lambda_{\max} = 535$ nm, giving rise the onset of optical absorption at nearly 1.7 eV. As it is already reported, this new band is attributed to the charge transfer [51]. In fact, photo-excitation begins in the polymer matrix and after electron diffusion; electron can be easily transferred to the SWCNTs as it reported for some polymer/SWCNTs nano-composites [52]. This charge transfer is the major parameter for which the improvement of photovoltaic characteristics is referred [53].

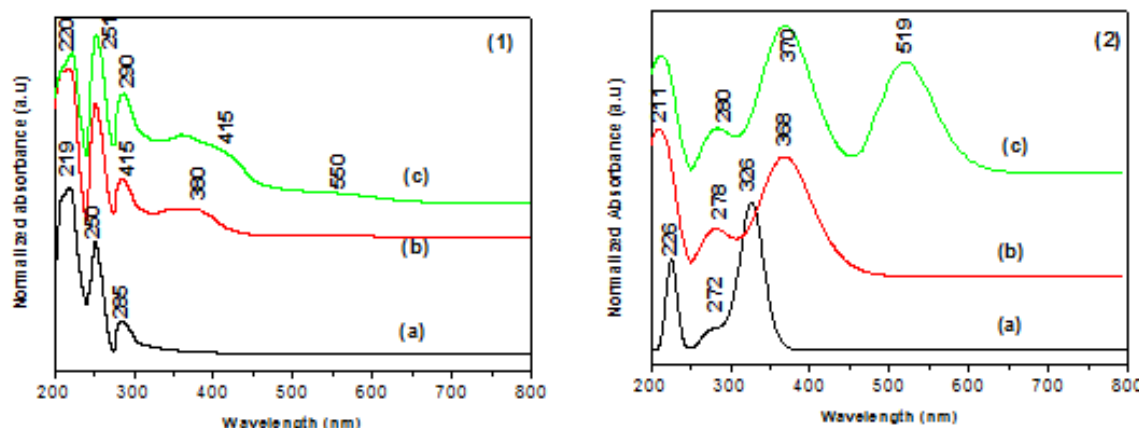


Figure 5: (1) Experimental (1) and theoretical (2) optical absorption spectra (a) PANIEB, (b) of sulfonic acid doped PANI and of the resulting nano-composite (c).

By referring to the experimental spectra, theoretically, optical absorption spectra relative to the neutral, doped or functionalized with SWCNTs states show also that same transitions are found, except a shifting. The observed shifting is probably due to the fact that calculations are done in gaseous phase and without inter-chain interaction. The above presented experimental results and the obtained theoretical calculations supports the modeling structure and consequently the grafting process which take place in the nitrogen atom.

In other hand and in order to evaluate the most appropriate SWCNTs weight concentration, which permits to evaluate the most appropriate photovoltaic characteristics, figure 6 represents the evolution of optical absorption spectra as a function of SWCNTs contents. First, it is clearly seen that sulfonic acid doping induces the creation of new additional band centered at $\lambda_{\max} = 340$ nm which show a progressive broadness. This latter is progressively red-shifted as a function of SWCNTs weight concentrations to be centered at 392 nm for both higher SWCNTs weight concentrations (2.16 % and 5.0 %). Moreover,

localized states due to the charge transfer creation within the energy gap are clearly seen after SWCNTs functionnalization [54], as shown, by the appearing of new additional feature in the wavelength ranging from 500 to 650 nm. In order to evaluate the effect of either acid doping or SWCNTs adding on the electronic structure of the basic material, the evolution of the optical energy gap and those of localized state the most significant parameters.

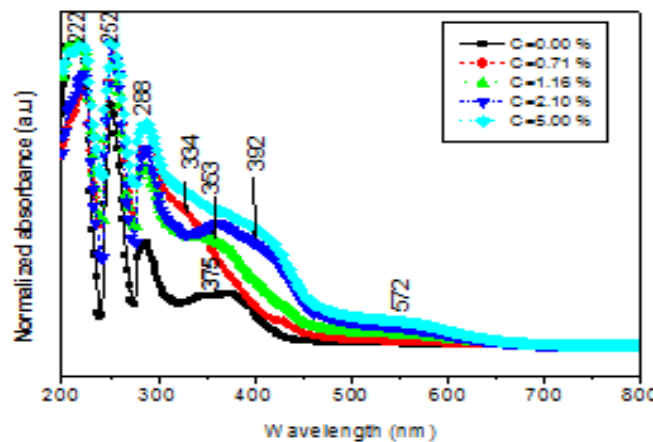


Figure 6: Variation of optical absorption spectra of doped PANI/SWCNTs composite versus the SWCNTs concentration

The band gap all compounds presented in this study has been estimated from the absorbance coefficient data as a function of wavelength using Tauc relation as given by equation 1 (Eq. 1) [55].

$$\alpha h\nu = B(h\nu - E_g)^n \quad (\text{Eq. 1})$$

Where α is the absorption coefficient, $h\nu$ is the photon energy, B is the band gap tailing parameter, E_g is the optical band gap and n is the transition probability index. By the plot of $(\alpha h\nu)^{1/2}$ versus $h\nu$ (figure 7-1), the energy gap is estimated by extrapolation of the linear dependence which occurs generally in the absorption onset [56, 57]. From figure 6, it is also noted that when SWCNTs are added a new feature appears in wavelength ranging from 500 to 650 nm. This new band which is progressively more pronounced when SWCNTs increase traduces the creation of localized states within the energy gap. In fact in the low photon energy range, the spectral dependence of the absorption coefficient (α) and photon energy ($h\nu$) is known as Urbach empirical rule, which is given by the following equation (Eq. 2) [58]:

$$\alpha = \alpha_0 \exp(-\frac{h\nu}{E_U}) \quad (\text{Eq. 2})$$

where α_0 is a constant and E_U denotes the energy of the band tail or sometimes called Urbach energy [57], which is weakly dependent upon temperature and is often interpreted as the width of the band tail due to localized states in the normally band gap that is associated with the disordered or low crystalline materials [58, 59]. Taking the logarithm of the two sides of Eq. 2, hence one can get a straight line equation (Eq. 3). Therefore, the band tail energy or Urbach energy (E_U) can be obtained from the slope of the straight line of plotting $\ln(\alpha)$ against the incident photon energy ($h\nu$) (Figure 7-2)

$$\ln(\alpha) = \ln(\alpha_0) + \frac{h\nu}{E_U} \quad (\text{Eq. 3})$$

All the data concerning the optical gap and the localized states are summarized in figure 7. The obtained energies gap for doped polyaniline is 2.863 eV. Then, when adding SWCNTs, this later takes the values of 2.48 eV for the lower SWCNTs concentrations and is typically the same (2.28 eV) for the other SWCNTs concentrations. The evolution of the optical gap as a function of SWCNTs concentrations presented on the onset of figure 7 demonstrates that it has a limit of 2.28 eV whatever are the SWCNTs concentrations. For the lower SWCNTs concentration (0.71), the new localized state which traduces the charge transfer creation has threshold energy of 1.7 eV. Starting from the 1.16 % Weight concentration the SWCS weight increase

has no significant effect on the energy position of localized states. Indeed, for all concentrations higher than 0.71 wt %, this threshold energy is typically 1.62 eV. The band width of localized states takes respectively 80 meV for the first SWCNTs concentration and nearly 65 meV for the other SWCNTs Concentrations.

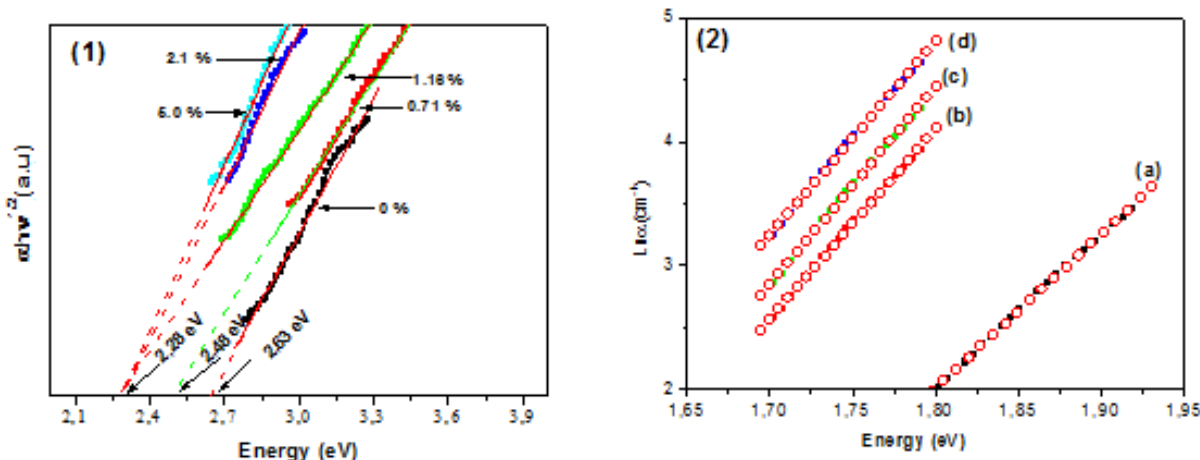


Figure 7: (1): Variation of $(\alpha h v)^{1/2}$ versus $h v$ in the onset of absorbance region, (2): Evaluation of band tail width of localized states as a function of SWCNTs weight concentrations.

The challenge is now to check the properties of this charge transfer availability between both components and to carry out the electronic properties of the resulting nano-composite [51]. The obtained electronic structure permits to elucidate the aptitude of the doped polyaniline on the photovoltaic conversion when the structure is regularly dispersed with SWCNTs to avoid an interpenetrating network. Principally, some electronic parameters such as HOMO, LUMO levels and ionization potential energy should be known. For these reasons and in order to evaluate the electronic structure of the used compounds, figure 8 represents the evolution of the HOMO-LUMO energies levels of both neutral and doped states for several units cells. Same procedure has been previously used in order to elucidate electronic affinity and ionization potential for infinite chain length [19].

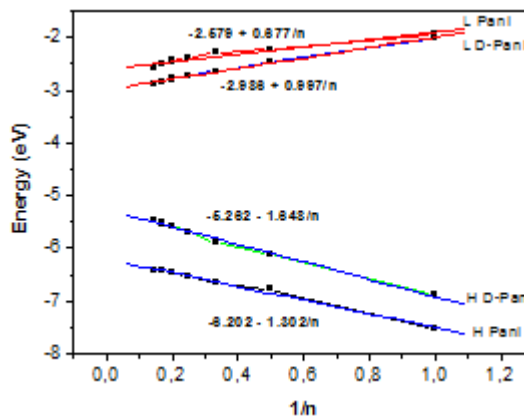


Figure 8: The evolution of the HOMO-LUMO energies levels of both neutral and doped states for several units cells (n).

As it is represented, these energetic levels show a linear relationship as a function of $1/n$. The extrapolation for infinite chains ($1/n \rightarrow 0$) permits to elucidate the corresponding electronic energy gap which

is evaluate to be 3.58 eV for polyaniline and 2.31 eV for the doped polyaniline. These values are in accordance with the already published experimental results [19]. The decrease of the electronic gap is evidently due to the creation of new energetic levels on the band gap of the neutral polymer as it is reported in the experimental part. In fact, for the doped polyaniline, the obtained energy value is lower than that obtained experimentally by nearly 0.5 eV. This difference can be related to the chain length diminution after sulfonic acid doping and to the weak inter-chain interaction due to the solvent state.

To more support this hypothesis concerning the charge transfer and the ability of electron or hole transport, figure 9 shows the contour plots of molecular orbitals (MOs) including HOMO and LUMO of both compounds.

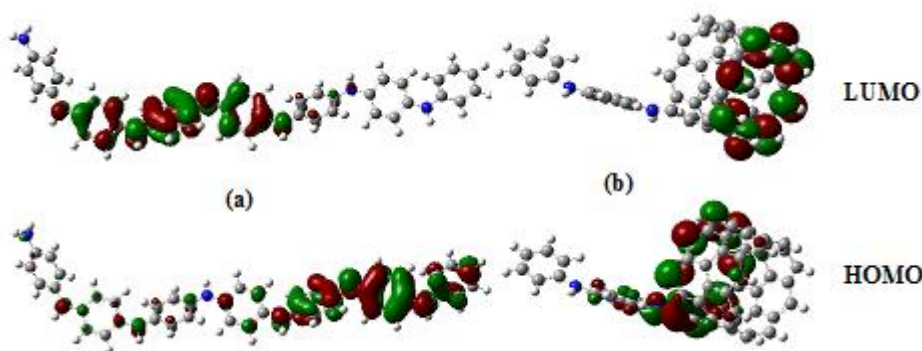


Figure 9: The contour plots of HOMO and LUMO orbitals of the studied compounds in their ground states: (a) doped polyaniline, (b) the nano-composite D-PANI/SWCNTs.

The HOMO possessed an anti-bonding p character between the two adjacent subunits [60]. However, the LUMO has a bonding character between the two subunits. When passing from ground to excited states, the HOMO state density was much localized on the donor moiety, while the electron density of LUMO was mainly localized on the acceptor moiety [61].

To evaluate the aptitude of the resulting interpenetrating network, on the photovoltaic conversion, some parameters should be checked such as the open-circuit voltage V_{OC} and the power conversion efficiency (PCE). These parameters are related by (Eq. 24) [62], where P_{in} is the incident power density and FF is the Field factor.

$$PCE = \frac{FF \cdot V_{OC} \cdot J_{SC}}{P_{in}} \quad (\text{Eq. 4})$$

The power conversion efficiency can also be checked theoretically from the Scharber diagram. This parameter is strictly related to the electronic structure of both components. In the other hand, as it is previously described [63], it is possible to evaluate the open-circuit voltage V_{OC} theoretically from the difference between HOMO and LUMO Energies levels of respectively donor and acceptor materials (Eq. 5):

$$V_{OC} (V) = \frac{1}{e} |E(\text{HOMO})^{\text{donor}} (\text{eV}) - |E(\text{LUMO})^{\text{acceptor}} (\text{eV})| - 0.3 (\text{V}) \quad (\text{Eq. 5})$$

Here e is the elementary charge and 0.3 V is a typical loss found in bulk hetero-junction solar cells due energy lost during the photo-charges generation [64]. A similar relation has been reported by Veldman et al., and Scharber et al. [65, 66]. For the SWCNTs alone, same calculations are also done on its modeling structure. Results give that SWCNTs exhibits HOMO and LUMO energy level respectively of 5.3 eV and 3.7 eV, by referring to vacuum level. These results are in good agreement with those recently reported [67]. By comparing

the obtained energetic levels for both doped polyaniline and SWCNTs to those of the work function of some metals, ITO and Al are the most appropriate for the architecture of the resulting solar cell (figure 10-a). From this electronic structure, the open circuit voltage (V_{oc}) is nearly 1.25 V.

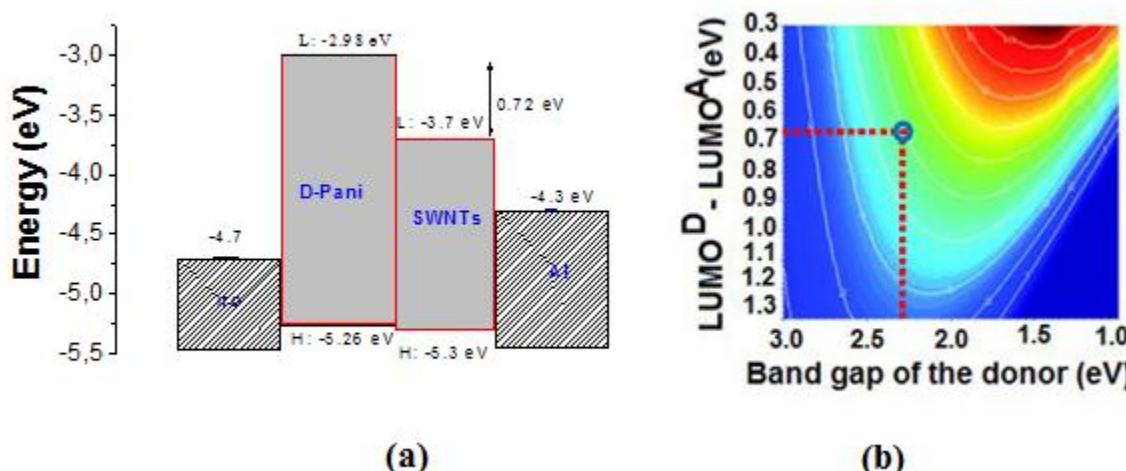


Figure 10: (a) Energetic diagram of the bulk hetero-junction ITO/Doped PANI/SWCNTs/Al photovoltaic cell (b) the power conversion efficiencies. D: Donor, A: Acceptor [64, 65].

As it is presented above in, localized states have the threshold energy of 1.62 eV. This energy coincides with those between HOMO of doped polyaniline and LUMO of SWCNTs energy levels. In fact, at this nanometer scale the transfer under illumination of electron between these energy levels is possible; especially for this interpenetrating network when the diffusion length is typically the same of chain length. Indeed, photo-excitation begins in the polymer matrix and finishes on the SWCNTs skeleton. Then, starting from the energy diagram of the resulting photovoltaic cell presented in figure 10-a, it is possible to estimate the maximum power conversion efficiency which is strictly based on from Scharber diagram (figure 10-b). The resulting interpenetrating network exhibits a power conversion efficiencies (PCEs) varying from the 4% to 5%. Note that the power conversion efficiency can be ameliorated by using short-oligo aniline rather than the polymer. However, the chain length (number of units) should be chosen as a function of its compatibility with the solar spectrum in the absorption process and as a function of the electron diffusion length [68].

Conclusions

Polyaniline EB is treated with sulfonic acid, and functionalized with SWCNTs. A systematic experimental study based on change of vibrational and optical properties is established as a function of SWCNTs contents. In the other hand, and by referring to the experimental conclusions, a theoretical study based on DFT calculations is also done in order to establish correlation structure-properties. Results show that a covalent bonding between doped polyaniline and SWCNTs is occurred via nitrogen link. This functionalization process induces the appearing of new broad band giving rise to a decrease of optical gap to reach the value of 2.28. The obtained nano-composite exhibits a good compatibility with the solar spectrum. Moreover, whatever the SWCNTs weight concentrations, a localized state within the gap having the threshold energy of 1.62eV is created. This localized state is the consequence of the donor-acceptor charge transfer. The modeling of the bulk hetero-junction photovoltaic cell ITO/D-PAN/SWCNTs/Al is also elucidated. The open voltage circuit is evaluated nearly 1.25 V and the corresponding power conversion efficiencies (PCEs) is estimated to be 4~ 5 %.

Acknowledgments- Le Centre de Recherches et des Technologies de l'Energie, Technopole Borj Cédria B.P N°95 – 2050, Hammam-Lif –Tunisie is gratefully acknowledged for his kind permission to use their facilities for the characterization.

References

1. Lizin S., Passel S. V., Schepper E. D., Vranken L., *Sol. Energy Mater. Sol. Cells.* 103 (2012) 1.
2. Deng P., Lei Y., Zheng X., Li S., Wu J., Zhu F., Ong B. S., Zhang Q., *Dyes Pigm.* 125 (2016) 407.
3. Tehrani Z., Korochkina T., Govindarajan S., Thomas D.J., Mahony J. O., Kettle J., Claypole T.C., Gethin D.T., *Org. Electron.* 26 (2015) 386.
4. Moaseri E., Karimi M., Baniadam M., M. Maghreb, *Composites Part A* 64 (2014) 228.
5. Mulligan C.J., Bilen C., Zhou X. , Belcher W.J., Dastoor P.C., *Sol. Energy Mater. Sol. Cells.* 133 (2015) 26.
6. Zhu H., Wei J., Wang K., Wu D., *Sol. Energy Mater. Sol. Cells.* 93 (2009) 1461.
7. Zaidi B., Bouzayen N., Wéry J., Alimi K., *J. Mol. Struct.* 971 (2010) 71.
8. Ferguson A. J., Blackburn J. L., Kopidakis N., *Mater. Lett.*, 90 (2013) 115.
9. Gao G. Yu, J., Hummelen J. C., Wudl F., Heeger A. J., *Sci.* 270 (1995) 1789.
10. Janssen R. A. J., Hummelen J. C., Sariciftci N. S., *MRS Bull.* 30 (2005) 33.
11. MacDiarmid A.G., *Synth. Met.* 84 (1997) 27.
12. Malinauskas A., *Polym.* 42 (2001) 3957.
13. Hundley M.F., Adams P.N., Mattes B.R., *Synth. Met.* 129 (2002) 291.
14. Huang J. J., Kaner R.B., *J. Am. Chem. Soc.* 126 (2004) 851.
15. Zhang L., Wan M., *Adv. Funct. Mater.* 13 (2003) 815.
16. Pinto N.J., Johnson A.T. J., MacDiarmid A.G., Mueller C. H., Theofylaktos N., Robinson D.C., Miranda F.A., *Appl. Phys. Lett.* 83 (2003) 4244.
17. Zhou Y., Freitag M., Hone J., Staii C., Johnson A.T. J., Pinto N.J., MacDiarmid A.G., *Appl. Phys. Lett.* 83 (2003) 3800.
18. Molapo K. M., Ndangili P. M., Ajayi R. F., Mbambisa G., Mailu S. M., Njomo N., Masikini M., Baker P., Iwuoha E. I., *Int. J. Electrochem. Sci.* 7 (2012) 11859.
19. Aleman C., Ferreira C. A., Torras J., Meneguzzi A., Canales M., Rodrigues M. A.S, Casanovas. J., *Polym.* 49, (2008) 5169.
20. Bejbouji H., Vignau L., Miane J. L., Dang M.-T., ElMostafa. O., Harmouchi M., Mouhsen A., *Sol. Energy Mater. Sol. Cells* 94 (2010) 176.
21. Pietro W.J., Franci M. M., Hehre W. J., Defrees D. J., Pople J. A. and Binkley J. S., *J. Am. Chem. Soc.* 104, (1982) 5039.
22. Pickholz M., dos Santos M.C., *Synth. Met.* 101 (1999) 528.
23. DiCesare N., Belletete M., Marrano C., Leclerc M., Durocher G., *J. Phys. Chem. A* 102 (1998) 5142.
24. Ayachi S., Alimi K., Bouachrine M., Hamidi M., Mevellec J.Y. and Porte J. P. L., *Synth. Met.* 156 (2006) 318.
25. Zou L. Y, Ren A. M, J. Feng K., X. Ran Q., Liu Y. L., Sun C. C., *Int. J. Quantum Chem.* 109 (2009) 1419.
26. Khoshkhologh M. J., Marsusi F., Abolhassani M. R., *Spectrochim. Acta, Part A* 136 (2015) 373.
27. Mbarek M., Zaidi B., Wéry J., Alimi K., *Synth. Met.* 1762 (2012) 162.
28. Ayachi S., Ghomrasni S. and Alimi K., *J. Appl. Polym. Sci.* 123 (2012) 2684.
29. Chiang J.-C., MacDiarmid A. G. , *Synth. Met.* 13(1986) 193.
30. Byron P. R., Hubert P., Salvetat J.-P., Zalamea L., *Compos. Sci. Technol.* 66, (2006) 1125.
31. Schroder E., Hyldgaard P., *Mater. Sci. Eng.*, C 23 (2003) 721.
32. Zaidi B., Ayachi S., Mabrouk A., Molinie P., Alimi K., *Polym. Degrad. Stab.* 79 (2003) 183.
33. Becke A.D., *J. Chem. Phys.* 98 (1993) 5648.
34. Pokrop R., Bajer I.K., Wielgus I., Zagorska M., Albertini D., Lefrant S., Louarn G., Pron A., *Synth. Met.* 159 (2009) 919.
35. Lee C., Yang W., Parr R.G., *Phys. Rev. B* 37 (1988) 785.
36. Gorelsky S.I., *Swizard Program*, University of Ottawa, Ottawa, Canada (2009)

37. Bourass. M. , Benjelloun. A. T., Benzakour. M., Mcharfi. M., Hamidi. M., Bouzzine. S.M., Serein-Spirau. F., Jarrosson. T., Lère-Porte J. P., Sotiropoulos. J. M., Bouachrine. M., *J. Mater. Environ. Sci.* 7 (2016) 700.
38. El Malki Z., Bouzzine S. M., Bejjit L., Haddad M., Hamidi M., Bouachrine M., *J. Appl. Polym. Sci.* 122, (2011) 3351.
39. Zhou X., Ren A.M., Feng J.K., *Polym.* 45 (2004) 7747.
40. M.J. Frisch, G.W. Trucks, H.B. Schlegel, G.E. Scuseria, M.A. Robb, J.R. Cheeseman, et al. Gaussian 09, revision B.01. Wallingford CT: *Gaussian, Inc.*; 2009.
41. Mishra A. K., Tandon P., *J. Phys. Chem. B*, 113 (2009) 14629.
42. Baibarac M., Baltog I., Lefrant S., Mevellec J.Y., Chauvet O., *Chem. Mater.* 15 (2003) 4149.
43. Pal G., Kumar S., *Prog. Aerosp. Sci.* 80 (2016) 33.
44. Lu X., Hu Y., Wang L., Guo Q., Chen Shu., Chen Sho., Hou H., Song Y., *Electrochim. Acta.* 189 (2016) 158.
45. Cosnier S., Holzinger M., *Electrochim. Acta.* 53 (2008) 3948.
46. Mishra A. K., Tandon P., *J. Phys. Chem. B* 113 (2009) 14629.
47. Wang Y., Zhang S., Deng Y. , *Mater. Lett.* 164 (2016) 132.
48. Chen B., Inoue S., Ando Y., *Diamond Relat. Mater.* 18, (2009) 975.
- 49 . Farag A. A. M., Ashery A., M. Abdel Rafea, *Synth. Met.* 160 (2010) 156.
50. Huang W.S., MacDiarmid A.G., *Polym.* 34 (1993) 1833.
51. Zaidi B., Bouzayen N., Wéry J., Alimi K., *Mater. Chem. Phys.* 126 (2011) 417.
52. Jeong D.-C., Song S. G., Satheeshkumar C., Lee Y., Kim K.-S., Song C., *Polym.* 69, (2015) 39.
53. He B., Tang Q., Luo J., Li Q., Chen X., Cai H., *J. Power Sources* 256, (2014) 170.
54. Goswami M., Ghosh R., Maruyama T., Meikap A. K., *Appl. Surf. Sci.* 364, (2016) 176.
55. Tauc J., Amorphous and Liquid Semiconductors, New York. *Plenum.*(1974).
56. Chithralekha P.,Subramanian E., Padiyan D. P. , *Sens. Actuators, B Chem.*122 (2007) 274.
57. Kumar A. ,*Nucl. Instrum. Methods Phys. Res., Sect. B* 269 (2011) 2798.
58. Urbach F., *Phys. Rev.B*, 92 (1953) 1324.
59. Kazmersky L. L. (Ed.), Polycrystalline and Amorphous Thin Films and Devices, *Academic Press*, New York, 135 (1980).
60. May V. and Kühn O., Charge and Energy Transfer Dynamics in Molecular Systems, 3rd Revised and Enlarged Edition Wiley, *VCH*, Berlin, (2011).
61. El Malki. Z., Bouachrine. M. , Hamidi. M. , Serein-Spirau. F., Lere-Porte. J. P., Sotiropoulos. J. M., *J. Mater. Environ. Sci.* 7 (9) (2016) 3244.
62. Mabrouk A., Azazi A., Alimi K., *Polym. Eng. Sci.* 53 (2013) 1040.
63. Gadisa A., Svensson M., Andersson M.R., Inganas O., *Appl. Phys. Lett.* 84 (2004) 1609.
64. Azazi A., Mabrouk A., Alimi K., *Comput. Theor. Chem.* 978 (2011) 7.
65. Veldman A., Meskers S.C.J., Janssen R. A. J., *Adv. Funct. Mater.* 19 (2009) 1939.
66. Scharber M.C., Sariciftci N.S. , *Prog. Polym Sci.* 38 (2013) 1929
67. Ferguson A. J., Belackburn J., Kopidakis N., *Mater. Lett.* 90 (2013) 115.
68. Zaidi B., Bouzayen N., Znaidia S. Mbarek M. et al. *J. Mol. Str.* 1039 (2013) 46.

(2016) ; <http://www.jmaterenvironsci.com/>